Journal of Molecular Spectroscopy 362 (2019) 69–76

Contents lists available at ScienceDirect

Journal of Molecular Spectroscopy

journal homepage: www.elsevier.com/locate/jms

MARVEL analysis of the measured high-resolution spectra of ^{14}NH

Daniel Darby-Lewis [a], Het Shah [b], Dhyeya Joshi [b], Fahd Khan [b], Miles Kauwo [b], Nikhil Sethi [b], Peter F. Bernath [c], Tibor Furtenbacher [d], Roland Tóbiás [d], Attila G. Császár [d], Jonathan Tennyson [a,*]

[a] Department of Physics and Astronomy, University College London, Gower Street, London WC1E 6BT, United Kingdom
[b] Preston Manor School, Carlton Avenue East, Wembley HA9 8NA, United Kingdom
[c] Department of Chemistry and Biochemistry, Old Dominion University, 4541 Hampton Boulevard, Norfolk, VA 23529, USA
[d] Institute of Chemistry, ELTE Eötvös Loránd University and MTA-ELTE Complex Chemical Systems Research Group, H-1518 Budapest 112, P.O. Box 32, Hungary

ARTICLE INFO

Article history:
Received 7 April 2019
In revised form 4 June 2019
Accepted 7 June 2019
Available online 12 June 2019

ABSTRACT

Rovibronic energy levels are determined for four low-lying electronic states ($X^3\Sigma^-$, $A^3\Pi$, $a^1\Delta$, and $c^1\Pi$) of the imidogen free radical (^{14}NH) using the MARVEL (Measured Active Rotational-Vibrational Energy Levels) technique. Compilation of transitions from both laboratory measurements and solar spectra, found in 18 publications, yields a dataset of 3002 rovibronic transitions forming elements of a measured spectroscopic network (SN). At the end of the MARVEL procedure, the majority of the transitions form a single, self-consistent SN component of 2954 rovibronic transitions and 1058 energy levels, 542, 403, and 58 for the $X^3\Sigma^-$, $A^3\Pi$, and $c^1\Pi$ electronic states, respectively. The $a^1\Delta$ electronic state is characterized by 55 Λ-doublet levels, counting each level only once. Electronic structure computations show that unusually the CCSD(T) method does not accurately predict the $a^1\Delta$ excitation energy even at the complete basis set limit.

1. Introduction

Imidogen, the NH free radical, is easily formed by flash photolysis of ammonia, often in excited electronic states [1,2]. The spectral signature of NH is observed in a variety of plasmas, including laser-produced ones in air [3] and liquids [4], those used for waste water treatment [5], and it also serves to measure ammonia concentration in plasmas [6]. Emissions can also be observed from NH trace species due to impurities in or seeding of fusion plasmas [7,8]. NH emissions are also observable in flames [9,10]. NH has also received considerable attention as an ultracold species that can be trapped using buffer gas cooling, magnetic trapping, or Zeeman relaxation [11–14] and has been the subject of detailed, state-resolved energy transfer experiments [15,16]. Lasing action has also been observed involving particular rovibronic states of NH [17].

NH is an important astronomical species, whose $A^3\Pi$–$X^3\Sigma^-$ spectrum was first recorded in the laboratory by Eder in 1893 [18]. This electronic transition has been detected in the Sun [19,20], in the comet Cunningham [21], in the interstellar medium by its absorption against various stars [22–25], and in the atmospheres of cool stars themselves [26]. The $c^1\Pi$–$a^1\Delta$ band system was originally observed by Dieke and Blue in 1934 [27] (see Fig. 1). Line lists are available which provide line strengths for rovibrational and rotational transitions within the $X^3\Sigma^-$ ground state of ^{14}NH [28,29] and for the $A^3\Pi$–$X^3\Sigma^-$ band system [30].

In this paper we analyse all the available high-resolution spectra of NH recorded in the laboratory [31–54] and obtained from spectroscopic observations of the Sun [54–56]. The purpose of this work is to provide accurate empirical energy levels with dependable uncertainties for ^{14}NH using the Measured Active Rotational-Vibrational Energy Levels (MARVEL) approach [57–60] (though the traditional name refers to rovibrational states, there is nothing in the original proposal of MARVEL [57] which prevents the use of rovibronic transitions in a MARVEL analysis). MARVEL energy levels have been used in the past to compute accurate, temperature-dependent ideal-gas thermodynamic data [61], to facilitate the empirical adjustment of potential energy surfaces [62], and to improve the accuracy of computed line lists [63,64].

The configuration of the ground electronic state of NH is $1\sigma^2 2\sigma^2 3\sigma^2 1\pi^2$. The doubly occupied π orbital gives rise to the $X^3\Sigma^-$ ground electronic state and the low-lying metastable excited $a^1\Delta$ and $b^1\Sigma^+$ states. Rearrangement of the electrons to $1\sigma^2 2\sigma^2 3\sigma^1 1\pi^3$ leads to two further low-lying electronic states designated $A^3\Pi$ and $c^1\Pi$. *Ab initio* calculations show that these are indeed the dominant configurations of these five electronic states [65,66]. Following some earlier studies [67,68], Owono Owono et al. [65] provide a comprehensive set of *ab initio* potential energy curves (PEC) for the states considered here. The work of Owono

* Corresponding author.
E-mail address: j.tennyson@ucl.ac.uk (J. Tennyson).

https://doi.org/10.1016/j.jms.2019.06.002
0022-2852/

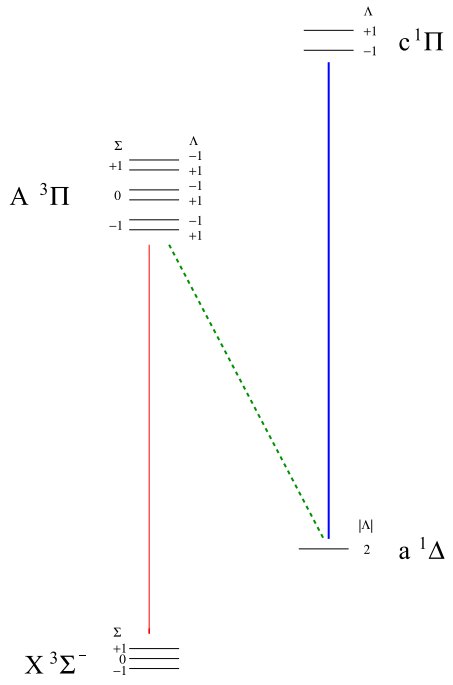

Fig. 1. Schematic representation of the three electronic band systems of NH analyzed in this work, with Hund's case *a* quantum numbers spin (Σ) and orbital (Λ) projections on the internuclear axis considered for each state separately; note that these quantum numbers are in general not good ones for NH. The total projection is given by $\Omega = |\Lambda + \Sigma|$. The spin-forbidden intercombination band system is depicted using a dashed line.

Owono et al. [65] is complemented by a high-accuracy study of the $X^3\Sigma^-$ ground-state PEC by Koput [69] and by other calculations [66].

This work started out by concentrating on the five lowest-lying electronic states of NH. However, although the metastable $b^1\Sigma^+$ state has been observed spectroscopically [1,34], there are insufficient data to warrant a MARVEL study including this state's energy levels. Analysis of this state therefore awaits the results of further laboratory measurements. Fig. 1 illustrates the electronic states and the electronic band systems of NH which we consider in this work. We also revisit the issue of obtaining accurate electronic exciation energies using standard quantum chemistry methods for this 8-electron system.

2. Methodological details

2.1. MARVEL

The MARVEL approach [57–60] enables a set of assigned experimental transition wavenumbers to be converted into empirical energy levels with associated uncertainties that are propagated from the input transitions to the output energy levels. This conversion relies on the construction of a spectroscopic network (SN) [70–73], which contains all measured and assigned interconnected transitions. For a detailed description of the approach, algorithm, and code, we refer the reader to Ref. [59].

The MARVEL approach has been used to validate compiled experimental rovibronic transitions for the astronomically important species $^{48}Ti^{16}O$ [74], which proved to be an important step in providing a greatly improved line list for TiO [75]. Although the spectroscopy of TiO is somewhat more complicated, there are similarities between this study and the one presented in Ref. [74]. Other MARVEL studies on chemically or astronomically important molecules include those for $^{12}C_2$ [76], $^{12}C_2H_2$ [77], $^{14}NH_3$ [78,79], three isotopologues of SO_2 [80], $H_2{}^{32}S$ [81], $^{90}Zr^{16}O$ [82], isotopologues of H_3^+ [83,84], and a series of investigations on isotopologues of water [60,85–90]. Note that the water studies provided the original motivation for developing the MARVEL procedure.

2.2. Quantum numbers

MARVEL requires that all transitions are assigned with a unique set of descriptors, usually quantum numbers, which are self-consistent across the entire dataset. Many studies considered here used Hund's case *b* quantum numbers for NH and these descriptors were adopted for this work. Each transition is therefore labeled by an electronic state label ($X^3\Sigma^-$, $A^3\Pi$, $a^1\Delta$, or $c^1\Pi$), a vibrational quantum number (v), the total angular momentum quantum number (J), the rotational angular momentum quantum number (N), and parity (e/f) [91]. For singlet states N is set equal to J.

Fig. 1 gives a schematic representation of the rovibronic band systems considered in this work; it also shows the spin (Σ) and orbital (Λ) angular momentum projections on the internuclear axis considered for each state. In the Hund's case *b* representation employed here these quantum numbers are not actually used.

In constructing a unified set of quantum numbers the following changes were made. The label F adopted for components of the $X^3\Sigma^-$ state by Bernath and co-workers [35,41,48,92,54] were mapped to the Hund's case *b* quantum number N as follows:

$$N = \begin{cases} J-1, & \text{if } F=1 \text{ and } p=e \\ J, & \text{if } F=2 \text{ and } p=f \\ J+1, & \text{if } F=3 \text{ and } p=e \end{cases} \quad (1)$$

The parity (p) of a rovibronic level incident to a rovibronic transition must satisfy one of the following relations:

$$\begin{aligned} \Delta J = 1: &\ e \leftrightarrow e \text{ or } f \leftrightarrow f, \\ \Delta J = 0: &\ e \leftrightarrow f. \end{aligned} \quad (2)$$

The interested reader should consult Fig. 1 of Dixon [93] for an explanation how the various notations represent the transitions within the $A^3\Pi$–$X^3\Sigma^-$ band system.

None of the studies considered here were able to resolve the Λ-doubling of the $a^1\Delta$ state where each (v,$J = N$) state should appear with either *e* or *f* parity. We decided to treat these (v,$J = N$) combinations as a single state and to adopt a parity label of *d* (for degenerate) in each case. This simplification means that odd-numbered cycles become possible in the experimental SN of ^{14}NH. In fact, while the great majority of the cycles within the minimum cycle basis [94] of the experimental SN of ^{14}NH have cycles of length four, the remaining cycles are largely split equally between cycles with length three and five. An example is the cycle formed by the transitions 27550.1873 [40] and 30826.5245 cm^{-1} [40] connecting the $a^1\Delta$ and $c^1\Pi$ states with the same upper rovibronic level, whereby the two lower rovibronic states are connected by the measured transition 3276.3820 cm^{-1} [39]. Validation of these odd-numbered cycles supports the assertion that Λ-doubling in the $a^1\Delta$ state is indeed small.

3. Compilation of experimental sources

^{14}NH has a pronounced hyperfine structure due to both ^{14}N ($I = 1$) and H ($I = \frac{1}{2}$) nuclear spins and most studies of its pure rotational spectrum resolve this structure. However, as none of the studies at higher wavenumbers resolve the hyperfine structure, it was decided not to consider hyperfine effects and treat the rotational spectra hyperfine unresolved. The hyperfine structure was therefore removed from sources 04LeBrWiSi [52], 82VaMeDy

[37], and 04FlBrMaOd [51]. Studies that only consider hyperfine transitions within a given (v, J, N) state [38,45] were excluded from our analysis at this stage. Averaging the hyperfine components, of course, leads to some loss of accuracy in the pure rotational levels for which it should be possible to obtain hyperfine-resolved energies. A number of older sources [1,32,33,95] were found to provide less accurate data than available from more recent measurements. These sources were not considered further.

Our preliminary analysis also showed that including the transition data of 82RaSa [36] caused conflicts within the SN. In 82RaSa [36] there are 70 measured lines in the $c^1\Pi$–$a^1\Delta$ band system in the range 27 105–27 697 cm^{-1} with a claimed uncertainty of about 0.005 cm^{-1}. Nearly all these lines were remeasured as part of a much more extended study by 86RaBe [40]. Removing six lines of 82RaSa [36] from the singlet subnetwork allowed the SN to form correctly once the average uncertainty had been increased to 0.03 cm^{-1}. We note that 82RaSa used a grating spectrograph and these measurements are essentially superseded by the more accurate Fourier transform spectroscopy (FTS) measurements of 86RaBe; these two datasets agree once the uncertainty for 82RaSa is increased. Remarkably, it was found necessary to remove only one further line, due to 86BrRaBe [41], during MARVEL's validation process.

Infrared spectra of the $X^3\Sigma^-$ state of ^{14}NH are also available from two distinct space-borne observations of solar spectra. The ATMOS [96] experiment, part of the Atmospheric Laboratory for Applications and Science (ATLAS) Space Shuttle program, provides solar spectra at a resolution of about 0.01 cm^{-1}. The Atmospheric Chemistry Experiment (ACE) [97] is a Canadian satellite mission which performs infrared solar occultation observations of the Earth's atmosphere producing detailed solar spectra in the infrared as a byproduct [98]. While the resolution of these spectra is lower than can be obtained in the laboratory, typically 0.01 cm^{-1} or lower, the high temperature of the Sun means that they probe rotational states not easily accessible in laboratory experiments. 91GeSaGrFa [56] used ATMOS to study pure rotational transitions of NH in the ground and first vibrationally excited states spanning levels with N from 20 to 42. 90GrLaSaVa [55] provides ATMOS R-branch spectra of the vibrational fundamental and the first hot band. However, these spectra do not resolve the fine structure splittings and there is only a single transition, the fundamental $R(N'' = 27)$ line, at 3389.147(10) cm^{-1}, which was not available from much higher resolution laboratory studies. As a result, we decided not to include transitions from 90GrLaSaVa [55] in our final compilation. Conversely, 10RaBe [54] analyses ACE spectra in the region of the vibrational fundamental where ACE gives much higher signal-to-noise ratio than ATMOS. 10RaBe also present laboratory spectra, so we divided their results into two segments and label them 10RaBe and 10RaBe_S2 to distinguish these independent subsets of data, with the latter source segment containing the less accurately measured transitions.

There are a number of studies of the intercombination band system which link the singlet and triplet subnetworks [49,50,99]. 99RiGe [49] used stimulated emission pumping of the strongly forbidden $a^1\Delta$ – $X^3\Sigma^-$ band system to study the singlet-triplet splitting. However, the data of 99RiGe [49] only have an accuracy of 0.1 cm^{-1} or worse and the source does not actually provide the primary transition data, so this source was not considered further. 03VaSaMoJo [50] used optical pumping to study $a^1\Delta$–$A^3\Pi$ transitions with an accuracy of 0.03 cm^{-1} or better. 03VaSaMoJo [50] also used the F labelling convention; therefore, their assignments were transformed as described above. Lower resolution experimental studies of the $a^1\Delta$–$X^3\Sigma^-$ emission spectra by 84RoSt [99] do not provide any transition wavenumbers and were not considered further.

4. Results and discussion

Table 1 presents a summary of the transitions data used in the final MARVEL run of this study. The latest version of the MARVEL code (`intMARVEL` [60]), with some minor modifications, was used to obtain the energy levels and the refined transitions. A total of 3002 assigned transitions from 18 distinct data sources were included in our final MARVEL analysis. Of these transitions and energy levels, 2954 and 1058, respectively, are contained within the principal component of the experimental SN of ^{14}NH linking levels in all four electronic states of interest. 48 transitions and

Table 1
Data source segments and some of their characteristics for the ^{14}NH molecule[a]

Segment tag	Band system	Range	A/V	ESU	ASU	MSU
97KlTaWi [47]	$X^3\Sigma^-$ – $X^3\Sigma^-$	31.570–33.356	3/3	3.00e−06	3.00e−06	3.00e−06
04FlBrMaOd [51]	$X^3\Sigma^-$ – $X^3\Sigma^-$	65.213–162.67	12/12	5.00e−06	5.00e−06	5.00e−06
07RoBrFlZi [53]	$X^3\Sigma^-$ – $X^3\Sigma^-$	28.977–156.21	34/34	1.00e−05	1.00e−05	1.00e−05
82VaMeDy [37]	$X^3\Sigma^-$ – $X^3\Sigma^-$	32.505–33.356	2/2	2.00e−05	7.54e−05	1.19e−04
86LeEvBr [42]	$X^3\Sigma^-$ – $X^3\Sigma^-$	98.495–98.495	1/1	2.00e−05	2.00e−05	2.00e−05
04LeBrWiSi [52]	$X^3\Sigma^-$ – $X^3\Sigma^-$	32.505–66.169	4/4	1.00e−04	1.84e−04	3.99e−04
86BoBrChGu [44]	$X^3\Sigma^-$ – $X^3\Sigma^-$	2310.1–3456.8	310/310	5.00e−04	7.82e−04	3.83e−03
82BeAm [35]	$X^3\Sigma^-$ – $X^3\Sigma^-$	2950.0–3293.1	29/29	1.00e−03	1.64e−03	5.28e−03
85HaAdKaCu [39]	$a^1\Delta$ – $a^1\Delta$	3177.9–3537.2	35/35	1.00e−03	3.86e−03	3.88e−02
86BrRaBe [41]	$A^3\Pi$– $X^3\Sigma^-$	26289–33080	1239/1238	1.00e−03	3.48e−03	4.11e−02
91GeSaGrFa [56]	X – $X^3\Sigma^-$	622.45–941.28	103/103	1.00e−03	4.16e−03	2.80e−02
99RaBeHi [48]	$X^3\Sigma^-$ – $X^3\Sigma^-$	2151.9–3459.0	500/500	1.00e−03	2.34e−03	2.63e−02
10RaBe [54]	$X^3\Sigma^-$ – $X^3\Sigma^-$	2151.8–2530.2	36/36	1.00e−03	1.00e−03	1.00e−03
10RaBe_S2 [54]	$X^3\Sigma^-$ – $X^3\Sigma^-$	2662.1–3459.0	266/266	5.00e−02	5.00e−02	5.00e−02
86UbMeTeDy [43]	$c^1\Pi$ – $a^1\Delta$	30059–30742	38/38	2.00e−03	5.57e−03	1.17e−02
03VaSaMoJo [50]	$A^3\Pi$– $a^1\Delta$	17002–17193	52/52	2.00e−03	1.10e−02	2.74e−02
86RaBe [40]	$c^1\Pi$ – $a^1\Delta$	26653–32938	250/250	3.00e−03	4.57e−03	3.85e−02
82RaSa [36]	$c^1\Pi$ – $a^1\Delta$	27106–27697	70/64	5.00e−03	2.64e−02	6.98e−02
90HaMi [46]	$c^1\Pi$ – $a^1\Delta$	21608–24525	18/18	2.00e−02	2.00e−02	2.00e−02

[a] Tags denote experimental data-source segments employed during this study (the identifier associated with the first segment of a data source, '_S1', is not written out explicitly). The column 'Range' indicates the range (in cm^{-1}) corresponding to validated wavenumber entries within the experimental linelist. 'A/V' is an ordered pair, where A and V are the number of assigned and validated transitions related to a given source segment, respectively, obtained at the end of the MARVEL analysis. ESU, ASU, and MSU designate the estimated, the average, and the maximum segment uncertainties in cm^{-1}, respectively. Rows of this table are arranged in the order of the ESUs with the restriction that the segments of the same data source should be listed one after the other.

62 energy levels could not be linked to the principal component, they are part of floating components, but they are retained in the dataset as they may be linked to the principal component when new experimental data become available.

After the reassignments and other manipulations considered in the last section, only 7 transitions had to be removed from the dataset considered by MARVEL as not consistent with the other transitions. These transitions are retained in the final transition list but are given as negative wavenumber entries.

The principal component of the experimental SN of ^{14}NH assembled during this study links together 1058 energy levels (see Fig. 2). Of these energy levels, 44, 818, 17 and 179 have resistances P^+, P^-, S, and U, respectively (definitions of the labels can be found in the ReadMe.txt file of the Supplementary Material). Energy levels with resistance P^+ are indeed dependable, while the others may change when even more accurate lines will be included in the database of experimental transitions. Although it is likely that even the non-P^+ energy levels are correct, especially those of P^-, they cannot be regarded as fully verified by the present analysis.

Due to the lack of truly high-accuracy first-principles energies for ^{14}NH, we used spectroscopic constants available in the literature to confirm the empirical (MARVEL) rovibrational energy levels derived during this study. For the $X^3\Sigma^-$ state, we used the PGOPHER [100] file of 15BrBeWe [29] to compute the rovibrational energy levels. Fig. 3 shows the differences between the MARVEL levels and this earlier work. As seen in Fig. 3, there are only few energy levels where the difference is larger than 0.05 cm^{-1} so the agreement is considered to be very good.

For the energy levels of the $a^1\Delta$ state, we used the molecular constants of 86RaBe [40], in the cases of $v = 0$ and 1, and 90HaMi [46] for $v = 2$ and 3. Prior to 1974 [101], no intercombination transitions could be measured; therefore, the energy separation of the singlet and triplet states of NH had to be estimated by indirect experimental data or by *ab initio* calculations. This is the reason why in 1963 McBride [102] set the value of $T_e(a^1\Delta)$ to 14922 cm^{-1} but in 1979, in their famous book, Huber and Herzberg [103] published 12566 cm^{-1} for this value, and 10 years later

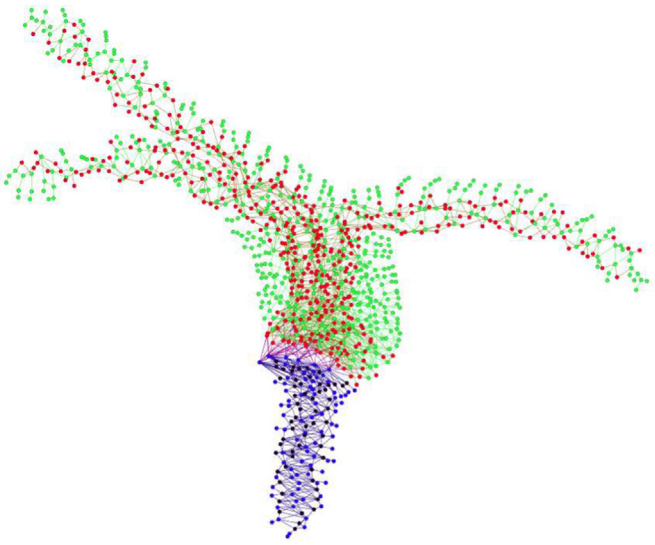

Fig. 2. The experimental spectroscopic network of the ^{14}NH molecule showing the different electronic states considered during this work with different color, red: $X^3\Sigma^-$, green: $A^3\Pi$, blue: $a^1\Delta$, and black: $a^1\Delta$. The relatively large number of bridges characterizing the spectroscopic network of ^{14}NH is evident from this figure. (For interpretation of the references to colour in this figure legend, the reader is referred to the web version of this article.)

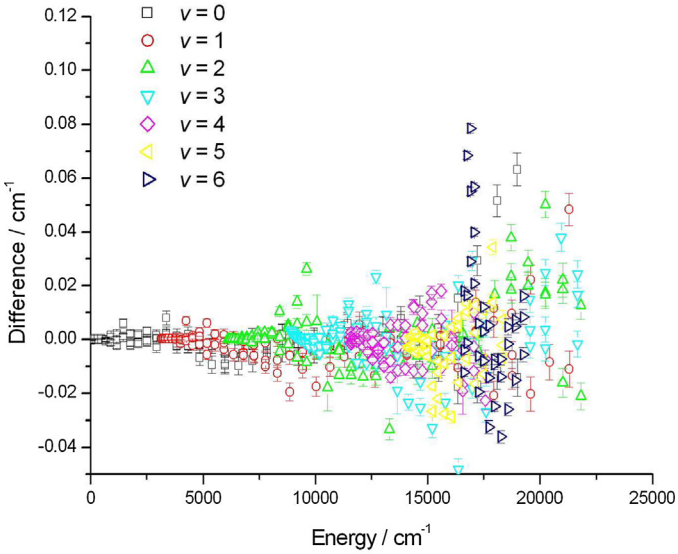

Fig. 3. Differences between the empirical MARVEL energy levels of this study and the earlier literature results of 15BrBeWe [29] related to the $X^3\Sigma^-$ electronic state.

Gurvich [104] used a value of 12577.1 cm^{-1} for T_e when calculating the thermochemical functions of the ^{14}NH molecule. The large shift in the T_0 value of the $a^1\Delta$ state over time can be explained by the pronounced multireference character of this state, due partly to the fact that it dissociates to an excited state of the N atom. The considerable difficulties the gold standard CCSD(T) level has in providing a correct estimate of $T_e(a^1\Delta)$ can be seen from the frozen-core and all-electron focal-point-analysis-type [105,106] entries of Table 2. The CCSD to CCSDT increment is huge and CCSD(T) can recover only less than half of this increment, a rather unusual situation. Though the CCSDTQ increment is not particularly large, it is unusually basis-set dependent, showing the necessity of a multireference treatment for obtaining the excitation energy of the $a^1\Delta$ state. The increments above CCSDTQ are very small, as usual and expected. Overall, the excitation energy is only about half of its unrestricted Hartree–Fock (UHF) estimate. One can estimate $T_e(a^1\Delta)$ starting from the all-electron CBS CCSDTQ value of Table 2, 12604(75) cm^{-1}, and adding to this the higher-order coupled-cluster estimates, −5(2) cm^{-1}, as well as the relativistic correction (computed at the all-electron aug-cc-pwCVQZ CCSD(T) level), −2 cm^{-1}. Adding the zero-point vibrational energy (ZPVE) correction, +27(5) cm^{-1}, obtained again at the aug-cc-pwCVQZ CCSD(T) level, yields our final $T_e(T_0)$ estimates of 12597(12624) cm^{-1}, with a conservative 2σ uncertainty estimate of ±80 cm^{-1}. These excitation energies support the best previous experimental estimates mentioned above.

The first high-accuracy measurement of the singlet-triplet splitting, between the $a^1\Delta$ ($v = 0$, $J = N = 2$) and $X^3\Sigma^-$ ($v = 0$, $J = 1$, $N = 0$) states, was obtained by 86RaBe [40], the value is 12688.39(10) cm^{-1}. This energy difference was given as 12687.8(1) cm^{-1} in 99RiGe [49] and probably the best value is given by 03VaSaMoJo [50], it is 12 688.622(4) cm^{-1}. The MARVEL value for this splitting is 12688.612(2) cm^{-1}. Since the T_e values are not accurate enough to confirm the MARVEL levels and there are no high-accuracy values for T_v in the literature, we fitted a simple Hamiltonian, taken from 86RaBe [40], for the degenerate energy levels of the $a^1\Delta$ state. We obtain the following values for $T_e + T_v$: 12655.761, 15838.558, 18875.218, and 21768.236 cm^{-1} for $v = 0$, 1, 2, and 3, respectively. Using these $T_e + T_v$ values and the rotational constants of 86RaBe [40] and 90HaMi [46], we could

Table 2
Focal-point-analysis table of the T_e excitation energy between the $X^3\Sigma^-$ and $a^1\Delta$ states of ^{14}NH.[a]

frozen-core	ΔE_e(UHF)	δ[MP2]	δ[CCSD]	δ[CCSD(T)]	δ[CCSDT]	δ[CCSDTQ]	δ[CCSDTQP]	δ[CCSDTQPH]	ΔE_e[FCI]
aug-cc-pwCVDZ	23 300.4	−3981.3	−2229.6	−1079.7	−1787.2	−148.6	−4.3	−0.0	14 069.9
aug-cc-pwCVTZ	23 222.7	−4838.1	−2043.0	−1078.9	−2002.3	−229.9	[−4.3]	[−0.0]	[11 947.3]
aug-cc-pwCVQZ	23 236.1	−5168.2	−1914.7	−1074.6	−2034.0	−247.7	[−4.3]	[−0.0]	[11 735.8]
aug-cc-pwCV5Z	23 240.9	−5316.0	−1836.4	−1074.9	−2039.4	–	[−4.3]	[−0.0]	[11 665.0]
CBS	**23 241.7(20)**	**−5471.1(500)**	**−1754.2(250)**	**−1075.3(10)**	**−2045.1(40)**	**−266.5(250)**]	[**−4.3(20)**]	[**−0.0(10)**]	**12 625.2(750)**
all-electron	ΔE_e(UHF)	δ[MP2]	δ[CCSD]	δ[CCSD(T)]	δ[CCSDT]	δ[CCSDTQ]	δ[CCSDTQP]		ΔE_e
aug-cc-pwCVDZ	23 300.4	−3995.9	−2133.8	−1093.6	−1846.8	−159.8	−4.9		14 065.6
aug-cc-pwCVTZ	23 222.7	−4823.6	−1924.2	−1089.4	−2100.5	−254.3	[−4.9]		
aug-cc-pwCVQZ	23 236.1	−5149.6	−1794.2	−1083.1	−2136.0	−276.0	[−4.9]		
aug-cc-pwCV5Z	23 240.9	−5296.1	−1716.1	−1082.6	–	–	[−4.9]		
CBS	**23 241.7(20)**	**−5449.9(500)**	**−1634.1(250)**	**−1082.0(20)**	**−2168.0(40)**	**−298.7(250)**	[**−4.9(20)**]		**12 604.1(750)**

[a] The symbol δ denotes the increment in the relative energy (ΔE_e) with respect to the preceding level of theory in the hierarchy HF → MP2 → CCSD → CCSD(T) → CCSDT → CCSDTQ → CCSDTQP → CCSDTQPH (≡ FCI in the case of the frozen-core approximation). CBS = complete basis set results (given in bold). The basis set extrapolations are based on the cardinal number X of the aug-cc-pCVXZ Gaussian basis-set family, for electron correlation increments they follow the formula X^{-3} and employ the largest two X values available. Uncertainties are given in parentheses. All energy values are given in cm^{-1}.

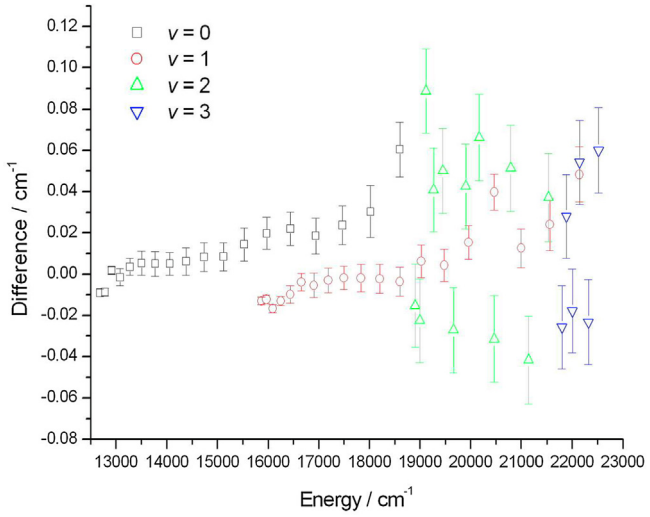

Fig. 4. Differences between the empirical MARVEL energy levels of this study and the earlier literature results of 86RaBe [40] and 90HaMi [46] related to the $a^1\Delta$ electronic state.

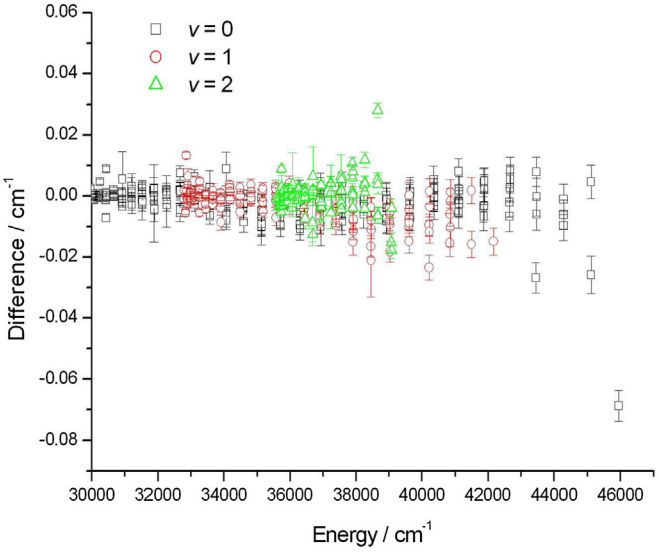

Fig. 5. Differences between the empirical MARVEL energy levels of this study and the earlier literature results of 10RaBe [54] related to the $A^3\Pi$ electronic state.

check the accuracy of the MARVEL energy levels. Fig. 4 shows the differences between the MARVEL levels and the effective Hamiltonian results. It can be seen that for the $v = 0$ and 1 vibrational states the agreement is nearly perfect, but in the cases of higher vibrational states the differences usually are larger than 0.03 cm^{-1}.

For checking the MARVEL energy levels of the $A^3\Pi$ state, we used the term values of 10RaBe [54]. The result of the comparison of the present empirical and the effective Hamiltonian energies can be seen in Fig. 5. Only two MARVEL energy levels could not be reproduced within 0.03 cm^{-1}.

We used the spectroscopic constants of 86RaBe [40] and our T_v values for the $c^1\Pi$ state to compute the energy levels of the $c^1\Pi$ state. Fig. 6 shows the result of this comparison: the agreement is almost perfect.

The list of MARVEL energy levels and the corresponding experimental transitions are placed in supplementary data.

Table 3 compares the vibrational band origins obtained during the MARVEL analysis with available experimental results. It is striking that direct vibrational band origin information is available only for the ground electronic state of ^{14}NH and only for $v = 1$–4 even though some experimental rovibrational data are available for v up to 6 in the $X^3\Sigma^-$ state, up to 3 in the $a^1\Delta$ state, up to 2 in the $A^3\Pi$ state, and for $v = 0$ and 1 in the $c^1\Pi$ state. It is also worth noting that the uncertainties obtained during the MARVEL

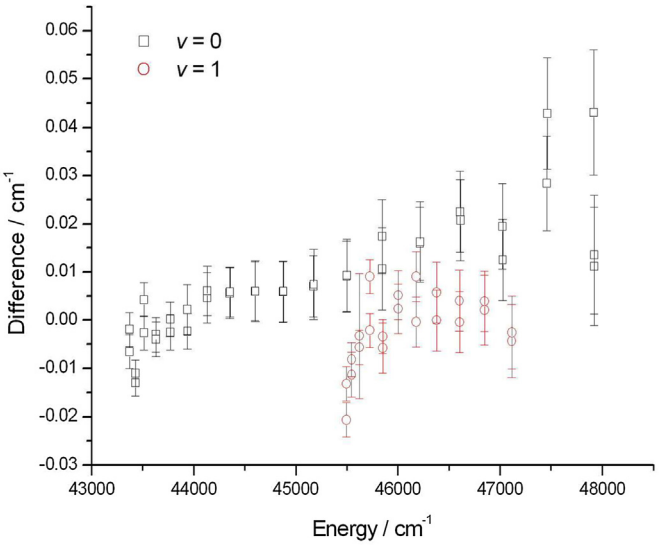

Fig. 6. Differences between the empirical MARVEL energy levels of this study and the earlier literature results of 86RaBe [40] related to the $c^1\Pi$ electronic state.

Table 3
Vibrational energy levels of ^{14}NH.[a]

ES	v	J	N	p	E(MARVEL)/cm^{-1}	E(86BoBrChGu [44])/cm^{-1}
$X^3\Sigma^-$	0	1	0	e	0	0
$X^3\Sigma^-$	1	1	0	e	3125.57241(50)	3125.57291(16)
$X^3\Sigma^-$	2	1	0	e	6094.87429(71)	6094.87502(20)
$X^3\Sigma^-$	3	1	0	e	8907.59729(87)	8907.59833(25)
$X^3\Sigma^-$	4	1	0	e	11562.3129(13)	11562.31434(42)

[a] ES = electronic state. The uncertainties of the reference data are calculated as the square root of the squared sum of the uncertainties found in Table 1 of Ref. [44].

analysis are slightly larger than the 1σ values reported in 86BoBrChGu [44]. Nevertheless, the agreement between MARVEL and 86BoBrChGu is excellent.

5. Conclusions

A Marvel analysis of the observed and assigned rovibronic transitions has been performed for the parent imidogen radical, ^{14}NH. After making a number of minor adjustments, a set of 1058 empirical rovibronic energy levels related to the principal component of the SN, containing 2954 validated transitions, are obtained for this radical spanning four low-lying electronic states. If desired, these energies provide suitable input for an effective Hamiltonian fit.

There are some high-resolution spectroscopic data available on higher-lying electronic states of NH including the $d^1\Sigma^+$ state [34,107] and various Rydberg states [108–110]. However, at this stage there are insufficient data available for any of these states to make their inclusion in a Marvel analysis productive. The ^{14}NH data produced here will be included in the newly formed Marvel project database [111] and can be actively updated should new high-resolution assigned spectra become available.

Finally, we note that a significant part of this work was performed by pupils from Preston Manor School in north-west London, as part of the ORBYTS (Original Research By Young Twinkle Students) project. Several other Marvel studies have been completed as part of the ORBYTS project, including those on ^{48}Ti^{16}O [74], acetylene [77], H_2S [81], ^{90}Zr^{16}O [82], and methane [112]. Sousa-Silva et al. [113] discusses our experiences of working with high-school students on high-level research projects. High-school students in Hungary were also involved in a Marvel analysis of the high-resolution spectra of $^{16}O_2$ [114].

Acknowledgement

We thank Dr. Ehsan Pedram of Preston Manor School for his considerable help during the course of this project. This work was supported by the Engineering and Physical Sciences Research Council (EPSRC) for a studentship for DD-L under grant EP/M507970/1. The work performed in Budapest received support from NKFIH (Grant No. K119658) and from the ELTE Excellence Program (1783-3/2018/FEKUTSTRAT) supported by the Hungarian Ministry of Human Capacities (EMMI). The collaboration between the Budapest and London groups received support from the European Cooperation in Science and Technology (COST) action CM1405, MOLIM: Molecules in Motion. Some support was provided by the NASA Laboratory Astrophysics program.

Appendix A. Supplementary material

Supplementary data associated with this article can be found, in the online version, at https://doi.org/10.1016/j.jms.2019.06.002.

References

[1] J. Masanet, A. Gilles, C. Vermeil, Light emission of the photofragments produced by photolysis of ammonia and ammonia-d_3 at 147, 123.6 and 104.8 nm: First observation of the $b^1\Sigma^+ - X^3\Sigma^-$ transition of NH and ND, J. Photochem. 3 (1974) 417–429.
[2] Y. Maruyama, T. Hikida, Y. Mori, Formation of NH ($A\ ^3\Pi_i$) in the flash photolysis of HN_3 at 121.6 nm. Role of N_2 triplet states, Chem. Phys. Lett. 116 (1985) 371–373.
[3] S.S. Harilal, B.E. Brumfield, M.C. Phillips, An evaluation of equilibrium conditions and temperature-dependent speciation in a laser-produced air plasma, Phys. Plasmas 25 (2018) 083303.
[4] R. Pflieger, T. Ouerhani, T. Belmonte, S.I. Nikitenko, Use of NH ($A\ ^3\Pi - X\ ^3\Sigma^-$) sonoluminescence for diagnostics of nonequilibrium plasma produced by multibubble cavitation, Phys. Chem. Chem. Phys. 19 (2017) 26272–26279.
[5] A. Hamdan, J.-L. Liu, M.S. Cha, Microwave plasma jet in water: characterization and feasibility to wastewater treatment, Plasma Chem. Plasma Proc. 38 (2018) 1003–1020.
[6] D. Zhang, Q. Gao, B. Li, J. Liu, Z. Li, Ammonia measurements with femtosecond laser-induced plasma spectroscopy, Appl. Opt. 58 (2019) 1210–1214.
[7] R. Perillo, R. Chandra, G.R.A. Akkermans, W.A.J. Vijvers, W.A.A.D. Graef, I.G.J. Classen, J. van Dijk, M.R. de Baar, Studying the influence of nitrogen seeding in a detached-like hydrogen plasma by means of numerical simulations, Plasma Phys. Controlled Fussion 60 (2018) 105004.
[8] E. Pawelec, T. Dittmar, A. Drenik, A. Meigs, J. Contributors, Molecular ND band spectroscopy in the divertor region of nitrogen seeded JET discharges, J. Phys. Conf. Ser. 959 (2018) 012009.
[9] C. Brackmann, E.J.K. Nilsson, J.D. Naucler, M. Alden, A.A. Konnov, Formation of NO and NH in NH_3-doped CH_4 + N_2 + O_2 flame: experiments and modelling, Combust. Flame 194 (2018) 278–284.
[10] N. Lamoureux, L. Gasnot, P. Desgroux, Quantitative NH measurements by using laser-based diagnostics in low-pressure flames, Proc. Combust. Inst. 37 (2019) 1313–1320.
[11] W.C. Campbell, E. Tsikata, H.-I. Lu, L.D. van Buuren, J.M. Doyle, Magnetic trapping and Zeeman relaxation of NH ($X\ ^3\Sigma^-$), Phys. Rev. Lett. 98 (2007) 213001.
[12] E. Tsikata, W.C. Campbell, M.T. Hummon, H.-I. Lu, J.M. Doyle, Magnetic trapping of NH molecules with 20 s lifetimes, New J. Phys. 12 (2010) 065028.
[13] A.O.G. Wallis, E.J.J. Longdon, P.S. Zuchowski, J.M. Hutson, The prospects of sympathetic cooling of NH molecules with Li atoms, Eur. Phys. J. D 65 (2011) 151–160.
[14] L.M.C. Janssen, A. van der Avoird, G.C. Groenenboom, Quantum reactive scattering of ultracold NH($X\ ^3\Sigma^-$) Radicals in a magnetic trap, Phys. Rev. Lett. 110 (2013) 063201.
[15] J.L. Rinnenthal, K.-H. Gericke, State-to-state energy transfer of NH ($X\ ^3\Sigma^-, v = 0, J, N$) in collisions with He and N_2, J. Chem. Phys. 116 (2002) 9776–9791.
[16] M. Kajita, Collision between magnetically trapped NH molecules in the ($N = 0, J = 1$) state, Phys. Rev. A 74 (3) (2006) 032710.
[17] J.H. Smith, D.W. Robinson, Pure rotational lasing in four electronic states of NH: impulsive to adiabatic collisional pumping, J. Chem. Phys. 71 (1979) 271–280.
[18] J.M. Eder, Contributions to spectral analysis, Denkschr. Wien Akad. 60 (1893) 1–24.
[19] A. Fowler, C.C.L. Gregory, The ultra-violet band of ammonia, and its occurrence in the solar spectrum, Proc. Roy. Soc. A 94 (1918) 470–471.
[20] N. Grevesse, A.J. Sauval, A study of molecular lines in the solar photospheric spectrum, Astron. Astrophys. 27 (1973) 29.
[21] P. Swings, T.C. Elvey, H.W. Babcoc, The spectrum of Comet Cunningham, 1940c, Astrophys. J. 94 (1941) 320–343.
[22] D.L. Lambert, R. Beer, Vibration-rotation bands of NH in the spectrum of alpha Orionis, Astrophys. J. 177 (1972) 541.
[23] D.M. Meyer, K.C. Roth, Discovery of interstellar NH, Astrophys. J. 376 (1991) L49–L52.
[24] I.A. Crawford, D.A. Williams, Detection of interstellar NH towards zeta Ophiuchi by means of ultra-high-resolution spectroscopy, Mon. Not. R. Astron. Soc. 291 (1997) L53–L56.
[25] T. Weselak, G.A. Galazutdinov, Y. Beletsky, J. Krelowski, Interstellar NH molecule in translucent sightlines, Mon. Not. R. Astron. Soc. 400 (2009) 392–397.

[26] W. Aoki, T. Tsuji, High resolution infrared spectroscopy of CN and NH lines: nitrogen abundance in oxygen-rich giants through K to late M, Astron. Astrophys. 328 (1997) 175–186.
[27] G.H. Dieke, R.W. Blue, A $^1\Pi \rightarrow {}^1\Delta$ band of NH and the corresponding ND band, Phys. Rev. 45 (1934) 395–400.
[28] J.S.A. Brooke, P.F. Bernath, C.M. Western, M.C. van Hemert, G.C. Groenenboom, Line strengths of rovibrational and rotational transitions within the X $^3\Sigma^-$ ground state of NH, J. Chem. Phys. 141 (2014) 054310.
[29] J.S.A. Brooke, P.F. Bernath, C.M. Western, Note: Improved line strengths of rovibrational and rotational transitions within the X $^3\Sigma^-$ ground state of NH, J. Chem. Phys. 143 (2015) 026101.
[30] A.M. Fernando, P.F. Bernath, J.N. Hodges, T. Masseron, A new linelist for the A $^3\Pi$ – X $^3\Sigma^-$ transition of the NH free radical, J. Quant. Spectrosc. Radiat. Transf. 217 (2018) 29–34.
[31] J. Malicet, J. Brion, H. Guenebau, Spectroscopic study of A$^3\Pi$(I) – X$^3\Sigma^+$S transition in NH radicals, J. Chim. Phys. Phys.-Chim. Biol. 67 (1970) 24.
[32] H.E. Radford, M.M. Litvakl, Imine (NH) detected by laser magnetic resonance, Chem. Phys. Lett. 34 (1975) 561–564.
[33] F.D. Wayne, H.E. Radford, Laser magnetic-resonance spectra of imine (NH) and its isotopes, Mol. Phys. 32 (1976) 1407–1422.
[34] W.R.M. Graham, H. Lew, Spectra of the d$^1\Sigma^+$ –c$^1\Pi$ and d$^1\Sigma$–b$^1\Sigma^+$ systems and dissociation energy of NH and ND, Can. J. Phys. 56 (1978) 85–99.
[35] P.F. Bernath, T. Amano, Difference frequency laser spectroscopy of the $v = 1 - 0$ transition of NH, J. Mol. Spectrosc. 95 (1982) 359–364.
[36] D.A. Ramsay, P.J. Sarre, The c$^1\Pi$ – a$^1\Delta$ system of the NH molecule, J. Mol. Spectrosc. 93 (1982) 445–446.
[37] F.C. Van den Heuvel, W.L. Meerts, A. Dymanus, Rotational hyperfine spectrum of the NH radical around 1 THz, Chem. Phys. Lett. 92 (1982) 215–218.
[38] W. Ubachs, J.J. ter Meulen, A. Dymanus, High-resolution laser spectroscopy on the A$^3\Pi$ – X$^3\Sigma^-$ transition of NH, Can. J. Phys. 62 (1984) 1374–1391.
[39] J.L. Hall, H. Adams, J.V.V. Kasper, R.F. Curl, F.K. Tittel, Color-center laser kinetic spectroscopy: observation of the a$^1\Delta$ NH vibrational fundamental, J. Opt. Soc. Am. B 2 (1985) 781–785.
[40] R.S. Ram, P.F. Bernath, Fourier-transform spectroscopy of NH: the c $^1\Pi$ – a $^1\Delta$ transition, J. Opt. Soc. Am. B 3 (1986) 1170–1174.
[41] C.R. Brazier, R.S. Ram, P.F. Bernath, Fourier transform spectroscopy of the A$^3\Pi$ – X$^3\Sigma^-$ transition of NH, J. Mol. Spectrosc. 120 (1986) 381–402.
[42] K.R. Leopold, K.M. Evenson, J.M. Brown, Far infrared laser magnetic resonance detection of NH and ND (a$^1\Delta$), J. Chem. Phys. 85 (1986) 324–330.
[43] W. Ubachs, G. Meyer, J.J. Ter Meulen, A. Dymanus, High-resolution spectroscopy on the c$^1\Pi$ – a$^1\Delta$ transition in NH, J. Mol. Spectrosc. 115 (1986) 88–104.
[44] D. Boudjaadar, J. Brion, P. Chollet, G. Guelachvilli, M. Vervloet, Infrared-emission spectra of 5 $\Delta v = 1$ sequence bands of the free-radical NH in its X$^3\Sigma^-$ state, J. Mol. Spectrosc. 119 (1986) 352–366.
[45] E.C.C. Vasconcellos, S.A. Davidson, J.M. Brown, K.R. Leopold, K.M. Evenson, Rotational and hyperfine constants of vibrationally excited NH(a$^1\Delta$; $v = 1$), J. Mol. Spectrosc. 122 (1987) 242–245.
[46] W. Hack, T. Mill, Spectroscopic constants of NH(a$^1\Delta$) from the c$^1\Pi(v' = 0)$ - a$^1\Delta(v \leqslant 3)$ laser-induced fluorescence spectra, J. Mol. Spectrosc. 144 (1990) 358–365.
[47] T. Klaus, S. Takano, G. Winnewisser, Laboratory measurement of the $N = 1 - 0$ rotational transition of NH at 1 THz, Astrophys. J. 322 (1997) L1–L4.
[48] R.S. Ram, P.F. Bernath, K.H. Hinkle, Infrared emission spectroscopy of NH: comparison of a cryogenic echelle spectrograph with a Fourier transform spectrometer, J. Chem. Phys. 110 (1999) 5557–5563.
[49] J.L. Rinnenthal, K.-H. Gericke, Direct high-resolution determination of the singlet–triplet splitting in NH using stimulated emission pumping, J. Mol. Spectrosc. 198 (1999) 115–122.
[50] S.Y.T. van de Meerakker, B.G. Sartakov, A.P. Mosk, R.T. Jongma, G. Meijer, Optical pumping of metastable NH radicals into the paramagnetic ground state, Phys. Rev. A 68 (2003) 032508.
[51] J. Flores-Mijangos, J.M. Brown, F. Matsushima, H. Odashima, K. Takagi, L.R. Zink, K.M. Evenson, The far-infrared spectrum of the ^{14}NH radical in its X $^3\Sigma^-$ state, J. Mol. Spectrosc. 225 (2004) 189–195.
[52] F. Lewen, S. Brünken, G. Winnewisser, M. Šimečková, Š. Urban, Doppler-limited rotational spectrum of the NH radical in the 2 THz region, J. Mol. Spectrosc. 226 (2004) 113–122.
[53] A. Robinson, J. Brown, J. Flores-Mijangos, L. Zink, M. Jackson, Spectroscopic study of the ^{14}NH radical in vibrationally excited levels of the X $^3\Sigma^-$ state by far infrared laser magnetic resonance, Mol. Phys. 105 (2007) 639–662.
[54] R.S. Ram, P.F. Bernath, Revised molecular constants and term values for the X $^3\Sigma^-$ and A $^3\Pi$ states of NH, J. Mol. Spectrosc. 260 (2010) 115–119.
[55] N. Grevesse, D.L. Lambert, A.J. Sauval, E.F. Van Dishoeck, C.B. Farmer, R.H. Norton, Identification of solar vibration-rotation lines of NH and the solar nitrogen abundance, Astron. Astrophys. 232 (1990) 225–230.
[56] M. Geller, C.B. Farmer, R.H. Norton, A.J. Sauval, N. Grevesse, First identification of pure rotation lines of NH in the infrared solar spectrum, Astron. Astrophys. 249 (1991) 550–552.
[57] T. Furtenbacher, A.G. Császár, J. Tennyson, MARVEL: measured active rotational-vibrational energy levels, J. Mol. Spectrosc. 245 (2007) 115–125.
[58] A.G. Császár, G. Czakó, T. Furtenbacher, E. Mátyus, An active database approach to complete rotational–vibrational spectra of small molecules, Annu. Rep. Comput. Chem. 3 (2007) 155–176.
[59] T. Furtenbacher, A.G. Császár, MARVEL: measured active rotational-vibrational energy levels. II. Algorithmic improvements, J. Quant. Spectrosc. Radiat. Transf. 113 (2012) 929–935.
[60] R. Tóbiás, T. Furtenbacher, J. Tennyson, A.G. Császár, Accurate empirical rovibrational energies and transitions of $H_2{}^{16}O$, Phys. Chem. Chem. Phys. 21 (2019) 3473–3495.
[61] T. Furtenbacher, T. Szidarovszky, J. Hruby, A.A. Kyuberis, N.F. Zobov, O.L. Polyansky, J. Tennyson, A.G. Császár, Definitive high-temperature ideal-gas thermochemical functions of the $H_2{}^{16}O$ molecule, J. Phys. Chem. Ref. Data 45 (2016) 043104.
[62] P.A. Coles, R.I. Ovsyannikov, O.L. Polyansky, S.N. Yurchenko, J. Tennyson, Improved potential energy surface and spectral assignments for ammonia in the near-infrared region, J. Quant. Spectrosc. Radiat. Transf. 219 (2018) 199–212.
[63] O.L. Polyansky, A.A. Kyuberis, N.F. Zobov, J. Tennyson, S.N. Yurchenko, L. Lodi, ExoMol molecular line lists XXX: a complete high-accuracy line list for water, Mon. Not. R. Astron. Soc. 480 (2018) 2597–2608.
[64] X. Huang, D.W. Schwenke, T.J. Lee, Quantitative validation of Ames IR intensity and new line lists for $^{32/33/34}S^{16}O_2$, $^{32}S^{18}O_2$ and $^{16}O^{32}S^{18}O$, J. Quant. Spectrosc. Radiat. Transf. 225 (2019) 327–336.
[65] L.C. Owono Owono, N. Jaidane, M.G. Kwato Njock, Z. Ben Lakhdar, Theoretical investigation of excited and Rydberg states of imidogen radical NH: Potential energy curves, spectroscopic constants, and dipole moment functions, J. Chem. Phys. 126 (2007) 244302.
[66] Z. Song, D. Shi, J. Sun, Z. Zhu, Accurate spectroscopic calculations of the 12 Λ-S and 25 Ω states of the NH radical including the spin-orbit coupling effect, Comput. Theor. Chem. 1093 (2016) 81–90.
[67] S.V. O'Neil, H.F. Schaefer, Configuration interaction study of the X $^3\Sigma^-$, a $^1\Delta$, and b $^1\Sigma^+$ states of NH, J. Chem. Phys. 55 (1971) 394–401.
[68] W. Meyer, P. Rosmus, PNO–CI and CEPA studies of electron correlation effects. III. Spectroscopic constants and dipole moment functions for the ground states of the first-row and second-row diatomic hydrides, J. Chem. Phys. 63 (1975) 2356–2375.
[69] J. Koput, Ab initio ground-state potential energy function and vibration-rotation energy levels of imidogen, NH, J. Comput. Chem. 36 (2015) 1286–1294.
[70] A.G. Császár, T. Furtenbacher, Spectroscopic networks, J. Mol. Spectrosc. 266 (2011) 99–103.
[71] T. Furtenbacher, A.G. Császár, The role of intensities in determining characteristics of spectroscopic networks, J. Molec. Struct. 1009 (2012) 123–129.
[72] T. Furtenbacher, P. Árendás, G. Mellau, A.G. Császár, Simple molecules as complex systems, Sci. Rep. 4 (2014) 4654.
[73] P. Árendás, T. Furtenbacher, A.G. Császár, On spectra of spectra, J. Math. Chem. 54 (2016) 806–822.
[74] L.K. McKemmish, T. Masseron, S. Sheppard, E. Sandeman, Z. Schofield, T. Furtenbacher, A.G. Császár, J. Tennyson, C. Sousa-Silva, MARVEL analysis of the measured high-resolution spectra of $^{48}Ti^{16}O$, Astrophys. J. Suppl. 228 (2017) 15.
[75] L.K. McKemmish, T. Masseron, J. Hoeijmakers, V.V. Pérez-Mesa, S.L. Grimm, S. N. Yurchenko, J. Tennyson, ExoMol molecular linelists – XXXIII. The spectrum of titanium oxide, Mon. Not. R. Astron. Soc. (2019).
[76] T. Furtenbacher, I. Szabó, A.G. Császár, P.F. Bernath, S.N. Yurchenko, J. Tennyson, Experimental energy levels and partition function of the $^{12}C_2$ molecule, Astrophys. J. Suppl. 224 (2016) 44.
[77] K.L. Chubb, M. Joseph, J. Franklin, N. Choudhury, T. Furtenbacher, A.G. Császár, G. Gaspard, P. Oguoko, A. Kelly, S.N. Yurchenko, J. Tennyson, C. Sousa-Silva, MARVEL analysis of the measured high-resolution spectra of C_2H_2, J. Quant. Spectrosc. Radiat. Transf. 204 (2018) 42–55.
[78] A.R. Al Derzi, T. Furtenbacher, S.N. Yurchenko, J. Tennyson, A.G. Császár, MARVEL analysis of the measured high-resolution spectra of $^{14}NH_3$, J. Quant. Spectrosc. Radiat. Transf. 161 (2015) 117–130.
[79] T. Furtenbacher, P.A. Coles, J. Tennyson, A.G. Császár, Updated MARVEL energy levels for ammonia, J. Quant. Spectrosc. Radiat. Transf. (2019). to be submitted.
[80] R. Tóbiás, T. Furtenbacher, A.G. Császár, O.V. Naumenko, J. Tennyson, J.-M. Flaud, P. Kumard, B. Poirier, Critical evaluation of measured rotational-vibrational transitions of four sulphur isotopologues of $S^{16}O_2$, J. Quant. Spectrosc. Radiat. Transf. 208 (2018) 152–163.
[81] K.L. Chubb, O.V. Naumenko, S. Keely, S. Bartolotto, S. MacDonald, M. Mukhtar, A. Grachov, J. White, E. Coleman, S.-M. Hu, A. Liu, A.Z. Fazliev, E.R. Polovtseva, V.M. Horneman, A. Campargue, T. Furtenbacher, A.G. Császár, S.N. Yurchenko, J. Tennyson, MARVEL analysis of the measured high-resolution rovibrational spectra of H_2S, J. Quant. Spectrosc. Radiat. Transf. 218 (2018) 178–186.
[82] L.K. McKemmish, J. Borsovszky, K.L. Goodhew, S. Sheppard, A.F.V. Bennett, A. D.J. Martin, A. Singh, C.A.J. Sturgeon, T. Furtenbacher, A.G. Császár, J. Tennyson, MARVEL analysis of the measured high-resolution spectra of $^{90}Zr^{16}O$, Astrophys. J. Suppl. 867 (2018) 33.
[83] T. Furtenbacher, T. Szidarovszky, E. Mátyus, C. Fábri, A.G. Császár, Analysis of the rotational–vibrational states of the molecular ion H_3^+, J. Chem. Theory Comput. 9 (2013) 5471–5478.
[84] T. Furtenbacher, T. Szidarovszky, C. Fábri, A.G. Császár, MARVEL analysis of the rotational–vibrational states of the molecular ions H_2D^+ and D_2H^+, Phys. Chem. Chem. Phys. 15 (2013) 10181–10193.
[85] J. Tennyson, P.F. Bernath, L.R. Brown, A. Campargue, M.R. Carleer, A.G. Császár, R.R. Gamache, J.T. Hodges, A. Jenouvrier, O.V. Naumenko, O.L. Polyansky, L.S. Rothman, R.A. Toth, A.C. Vandaele, N.F. Zobov, L. Daumont, A.Z. Fazliev, T. Furtenbacher, I.E. Gordon, S.N. Mikhailenko, S.V. Shirin, IUPAC critical evaluation of the rotational-vibrational spectra of water vapor. Part I.

Energy levels and transition wavenumbers for $H_2{}^{17}O$ and $H_2{}^{18}O$, J. Quant. Spectrosc. Radiat. Transf. 110 (2009) 573–596.
[86] J. Tennyson, P.F. Bernath, L.R. Brown, A. Campargue, M.R. Carleer, A.G. Császár, L. Daumont, R.R. Gamache, J.T. Hodges, O.V. Naumenko, O.L. Polyansky, L.S. Rothman, R.A. Toth, A.C. Vandaele, N.F. Zobov, A.Z. Fazliev, T. Furtenbacher, I. E. Gordon, S.N. Mikhailenko, B.A. Voronin, IUPAC critical evaluation of the rotational-vibrational spectra of water vapor. Part II. Energy levels and transition wavenumbers for $HD^{16}O$, $HD^{17}O$, and $HD^{18}O$, J. Quant. Spectrosc. Radiat. Transf. 111 (2010) 2160–2184.
[87] J. Tennyson, P.F. Bernath, L.R. Brown, A. Campargue, M.R. Carleer, A.G. Császár, L. Daumont, R.R. Gamache, J.T. Hodges, O.V. Naumenko, O.L. Polyansky, L.S. Rothmam, A.C. Vandaele, N.F. Zobov, A.R. Al Derzi, C. Fábri, A.Z. Fazliev, T. Furtenbacher, I.E. Gordon, L. Lodi, I.I. Mizus, IUPAC critical evaluation of the rotational-vibrational spectra of water vapor. Part III. Energy levels and transition wavenumbers for $H_2{}^{16}O$, J. Quant. Spectrosc. Radiat. Transf. 117 (2013) 29–80.
[88] J. Tennyson, P.F. Bernath, L.R. Brown, A. Campargue, A.G. Császár, L. Daumont, R.R. Gamache, J.T. Hodges, O.V. Naumenko, O.L. Polyansky, L.S. Rothmam, A.C. Vandaele, N.F. Zobov, N. Dénes, A.Z. Fazliev, T. Furtenbacher, I.E. Gordon, S.-M. Hu, T. Szidarovszky, I.A. Vasilenko, IUPAC critical evaluation of the rotational-vibrational spectra of water vapor. Part IV. Energy levels and transition wavenumbers for $D_2{}^{16}O$, $D_2{}^{17}O$ and $D_2{}^{18}O$, J. Quant. Spectrosc. Radiat. Transf. 142 (2014) 93–108.
[89] J. Tennyson, P.F. Bernath, L.R. Brown, A. Campargue, A.G. Császár, L. Daumont, R.R. Gamache, J.T. Hodges, O.V. Naumenko, O.L. Polyansky, L.S. Rothman, A.C. Vandaele, N.F. Zobov, A database of water transitions from experiment and theory (IUPAC Technical Report), Pure Appl. Chem. 86 (2014) 71–83.
[90] T. Furtenbacher, J. Tennyson, O.V. Naumenko, O.L. Polyansky, N.F. Zobov, A.G. Császár, The 2018 update of the IUPAC database of water energy levels, J. Quant. Spectrosc. Radiat. Transf. 25 (2019). In preparation.
[91] J.M. Brown, J.T. Hougen, K.P. Huber, J.W.C. Johns, I. Kopp, H. Lefebvre-Brion, A. J. Merer, D.A. Ramsay, J. Rostas, R.N. Zare, Labeling of parity doublet levels in linear molecules, J. Mol. Spectrosc. 55 (1975) 500–503.
[92] R.S. Ram, P.F. Bernath, Fourier transform infrared emission spectroscopy of ND and PH, J. Mol. Spectrosc. 176 (1996) 329–336.
[93] R.N. Dixon, The $0-0$ and $1-0$ bands of the $A^3\Pi_i - X^3\Sigma^-$ system of NH, Can. J. Phys. 37 (1959) 1171.
[94] R. Tóbiás, T. Furtenbacher, A.G. Császár, Cycle basis to the rescue, J. Quant. Spectrosc. Rad. Transfer 203 (2017) 557–564.
[95] G. Krishnamurty, N.A. Narasimham, Predissociations in the d $^1\Sigma^-$ - c $^1\Pi$ bands of NH, J. Mol. Spectrosc. 29 (1969) 410–414.
[96] M. Abrams, A. Goldman, M. Gunson, C. Rinsland, R. Zander, Observations of the infrared solar spectrum from space by the ATMOS experiment, Appl. Opt. 35 (1996) 2747–2751.
[97] P.F. Bernath, The Atmospheric Chemistry Experiment (ACE), J. Quant. Spectrosc. Radiat. Transf. 186 (2017) 3–16.
[98] F. Hase, L. Wallace, S.D. McLeod, J.J. Harrison, P.F. Bernath, The ACE-FTS atlas of the infrared solar spectrum, J. Quant. Spectrosc. Radiat. Transf. 111 (2010) 521–528.
[99] F. Rohrer, F. Stuhl, NH (a $^1\Delta$ – X $^3\Sigma^-$) emission from the gas-phase photolysis of HN_3, Chem. Phys. Lett. 111 (1984) 234–237.
[100] C.M. Western, PGOPHER: A program for simulating rotational, vibrational and electronic spectra, J. Quant. Spectrosc. Radiat. Transf. 186 (2017) 221–242.
[101] A. Gilles, J. Masanet, C. Vermeil, Direct determination of the NH b $^1\Sigma^+$ – X $^3\Sigma^-$ energy difference, Chem. Phys. Lett. 25 (1974) 346–347.
[102] B. McBride, Thermodynamic Properties to 6000 degrees K for 210 substances involving the first 18 elements, National Aeronautics and Space Administration special paper, Office of Scientific and Technical Information, National Aeronautics and Space Administration, 1963. https://books.google.hu/books?id=o3WGHAAACAAJ.
[103] K. Huber, G. Herzberg, Molecular Spectra and Molecular Structure IV Constants of Diatomic Molecule, Van Nostrand Reinhold Company, New York, 1979.
[104] L.V. Gurvich, I.V. Veyts, C.B. Alcock (Eds.), Thermodynamic Properties of Individual Substances, Part Two: Tables, Vol. 1, Hemisphere Publishing Corporation, New York, 1989.
[105] W.D. Allen, A.L.L. East, A.G. Császár, Ab initio anharmonic vibrational analyses of non-rigid molecules, in: J. Laane, M. Dakkouri, B. van der Veken, H. Oberhammer (Eds.), Structures and Conformations of Nonrigid Molecules, Kluwer, Dordrecht, 1993, pp. 343–373.
[106] A.G. Császár, W.D. Allen, H.F. Schaefer III, In pursuit of the ab initio limit for conformational energy prototypes, J. Chem. Phys. 108 (1998) 9751–9764.
[107] M.N.R. Ashfold, S.G. Clement, J.D. Howe, C.M. Western, Resonance-enhanced multiphoton ionisation spectroscopy of the NH (ND) radical. Part 1. The d $^1\Sigma^+$ state, J. Chem. Soc. Faraday Trans. 87 (1991) 2515–2523.
[108] S.G. Clement, M.N.R. Ashfold, C.M. Western, Resonance-enhanced multiphoton ionisation spectroscopy of the NH (ND) radical. Part 2.-Singlet members of the 3p Rydberg complex, J. Chem. Soc. Faraday Trans. 88 (21) (1992) 3121–3128.
[109] S.G. Clement, M.N.R. Ashfold, C.M. Western, R.D. Johnson III, J.W. Hudgens, Triplet rydberg states of the imidogen radical characterized via two-photon resonance-enhanced multiphoton ionization spectroscopy, J. Chem. Phys. 97 (1992) 7064–7072.
[110] S.G. Clement, M.N.R. Ashfold, C.M. Western, E. de Beer, C.A. de Lange, N.P.C. Westwood, New singlet Rydberg states of the NH (ND) radical in the energy range 92 000–100 000 cm^{-1} characterized by resonance enhanced multiphoton ionization-photoelectron spectroscopy, J. Chem. Phys. 96 (1992) 4963–4973.
[111] T. Furtenbacher, A.G. Császár, J. Tennyson, et al., The MARVEL project, J. Quant. Spectrosc. Radiat. Transf. (2019). in preparation.
[112] E.J. Barton, M. Liu, T. Farnell, J. Tennyson, C. Sousa-Silva, V. Boudon, T. Furtenbacher, A.G. Császár, MARVEL analysis of the measured rotation-vibration spectra of methane, JQSRT (2019).
[113] C. Sousa-Silva, L.K. McKemmish, K.L. Chubb, J. Baker, E.J. Barton, M.N. Gorman, T. Rivlin, J. Tennyson, Original Research By Young Twinkle Students (ORBYTS): when can students start performing original research?, Phys Educ. 53 (2018) 015020.
[114] T. Furtenbacher, M. Horváth, D. Koller, P. Sólyom, A. Balogh, I. Balogh, A.G. Császár, MARVEL analysis of the measured high-resolution rovibronic spectra and definitive ideal-gas thermochemistry of the $^{16}O_2$ molecule, J. Phys. Chem. Ref. Data 48 (2019) 023101.